Design of Hollow Nanosphere Structured Polypyrrole/Sn and SnO$_2$ Nanoparticles by COP Approach for Enhanced Electron Transport Behavior

G. Sowmiya[1] · G. Velraj[2]

Abstract

In this report, the Polypyrrole, PPy/Sn and PPy/SnO$_2$ nanocomposites have been prepared through a facile chemical oxidation polymerization (COP) techniques. The resulting nanocomposites were characterized by Fourier transform-infrared spectroscopy (FT-IR), X-ray diffraction (XRD) and UV–Visible spectroscopy (UV–Vis). FTIR analysis confirms the presence of nano tin and SnO$_2$ particles in the molecular structure. XRD patterns revealed that the sample is crystallite nature with tetragonal structure. The average crystallite size for the PPy/SnO$_2$ and PPy/Sn nanocomposites are 27 and 56 nm. In addition to this, the surface morphologies and elemental compositions were investigated by field emission scanning electron microscopy (FESEM), high resolution transmission electron microscopy (HRTEM) and Energy-dispersive X-ray spectroscopy (EDX). We obtained the aggregate, hollow nanosphere for PPy/Sn nanocomposites. The results indicate that the hollow sphere of the nanocomposites effectively enhances the electrical conductivity.

Keywords COP approach · Hollow nanosphere · Polymer matrix · Electron transfer · AC electrical conductivity

1 Introduction

Recent years, the synthesis of electrically conducting polymers have been focused on the various polymers such as polypyrrole, polyaniline, polyacetylene and polythiophene as well as they initiate a huge range of applications as synthetic metals, as they can alternate for semiconductors and conductors in an enormous variety of electronic and electric devices [1–4]. Amongst plenty of conducting polymers (CPs), polypyrrole (PPy) is one of the most broadly investigated owing to its unique transport properties, facile synthesis, higher conductivity, good environmental and electrical stability [5]. Moreover PPy offers tremendous technological potential applications such as battery electrodes [6], biological sensors [7], corrosion protection [8], microwave shielding [9, 10] and sensors [11]. It can be easily produced under chemical and electrochemical conditions in special organic solvents and within aqueous solutions. Notably, the chemical synthetic procedures are typically focused on the formation of nanostructured polypyrrole materials [12–18]. A new class of materials emerged, known as composites, prepared by mixing properly with organic and inorganic base materials in appropriate form. The composite materials have individual properties, however as seen in some of the cases, they can also have few desirable properties from both the parent organic and inorganic class of materials. As a consequence, there are growing interests in combining both organic and inorganic materials for applications in electronics, optics, magnetism and etc. [19–21]. Nevertheless, metallic nanoparticles have been extensively deliberate because of their exacting importance in many applications. Moreover the metal oxide nano materials exhibit a high surface area to volume ratio and are thus expected to modify the optical and electrical properties of conducting polymers [22, 23]. Some efforts have been over with regard to the synthesis of conductive PPy or PANI with metal oxide nanocomposites such as MnO$_2$, TiO$_2$, NiO, ZnO, and Fe$_3$O$_4$ as electrode or hybrid materials with high capacitance and suitable performance for supercapacitor applications [24–30]. Recently, the large variety of metal nanoparticles, diverse methods for the

✉ G. Velraj
gvelraj@yahoo.co.uk

[1] Department of Physics, Periyar University, Salem 636 011, Tamilnadu, India

[2] Department of Physics, Anna University, Chennai 600 025, Tamilnadu, India

fabrication of tin nanoparticles have been often proposed [31–33]. A rutile tin oxide is an n-type semiconductor with a broad energy gap ($Eg = 3.62$ eV, at 300 K). It is mainly fascinating, because it has high chemical stability and excellent optical and electrical properties and has been extensively used as a catalyst for oxidation of organic compounds, and as gas sensors [34, 35], rechargeable Li-batteries, and optical electronic devices [36, 37]. On the otherhand, the inorganic core can be a metal or a metal oxide, and the organic shell can be a conducting polymer. Incorporation of inorganic fillers into conducting polymer matrices has also been studied, utilizing both chemical and electrochemical polymerization processes [38].

The present research work describes an efficient method to synthesize and characterization of pure PPy, PPy/SnO$_2$ and PPy/Sn nanocomposites was performed through chemical oxidative method at room temperature. The influence of SnO$_2$ and Sn nanoparticles coalesce with PPy matrix will provide an enhanced electrical conductivity. To our best of the knowledge no comparative study on the synthesis and performance of such materials has been presented so far. The molecular structure, crystalline, morphological, elemental composition, dielectric and AC electrical conductivity of synthesized samples were investigated in detail.

2 Experimental Methods

2.1 Materials

The pyrrole monomer (99.98% pure) Sigma Aldrich, K$_2$Cr$_2$O$_7$ (Sigma Aldrich), Sulfuric acid (H$_2$SO$_4$) (Merck), nano tin (98%) (Nano shell), Tin (IV) chloride (Merck), DDW (Double Distilled water) is used for all reactions. All the chemicals are of AR grade and are used without further purification.

2.2 Synthesis of Polypyrrole and SnO$_2$ Nanoparticles

The Polypyrrole was prepared by using chemical oxidative polymerization method. H$_2$SO$_4$ is used as a dopant (K$_2$Cr$_2$O$_7$) is used as an oxidant. The pyrrole monomer solution was stirred at ice temperature and H$_2$SO$_4$ solution was added drop wise into pyrrole monomer solution. The reaction mixture was stirred one hour at constant rpm value. The solution of 0.5 M of K$_2$Cr$_2$O$_7$ was added drop wise into the mixture.This reaction mixture kept under the ice temperature and stirred constant RPM value at 24 h continuously. The black precipitate was separated out by filtering. The final product was dried in laboratory oven at 100 °C for 90 min. Finally the product was ground into fine powder using mortar and pestle. Typically SnO$_2$ nanoparticles were synthesized by co-precipitation method, using SnCl$_2$ as a Sn source. Then 0.2 M of SnCl$_2$·2H$_2$O was dissolved in 200 ml of DDW. After that 6 ml of ammonia solution was added, and the mixture was stirred vigorously at room temperature for 1.5 h to form a precipitate. The white gel precipitate was allowed to settle for 14 h, collected by filtration and thoroughly rinsed with distilled water. The obtained precipitate was heated at 110 °C until dry, and then calcined at 500 °C for 5 h to yield SnO$_2$ nanoparticles.

2.3 Preparation of PPy/Sn and PPy/SnO$_2$ Nanocomposites

The particular amount of PPy powder was blended with 100 ml of distilled water and the mixture was added to 200 mg of nano tin particle and stirred constant RPM value at 12 h continuously. Then the precipitate was separated out by filtering. The final suspension was dried in an oven at 100 °C for 60 min. Similarly the same procedure was carried out for the PPy/SnO$_2$ nanocomposite instead of Sn nanoparticle.

3 Results and Discussion

3.1 FT-IR Spectral Analysis

The chemical structure of pure PPy, PPy/SnO$_2$ and PPy/Sn nanocomposites was confirmed by using FT-IR spectra are presented in Fig. 1a–c. The absorbance bands at 619 cm^{-1} and 617 cm^{-1} is due to the presence of antisymmetric Sn–O–Sn band, this peak clearly indicates the formation of SnO$_2$ and Sn nanoparticles on PPy/SnO$_2$ and PPy/
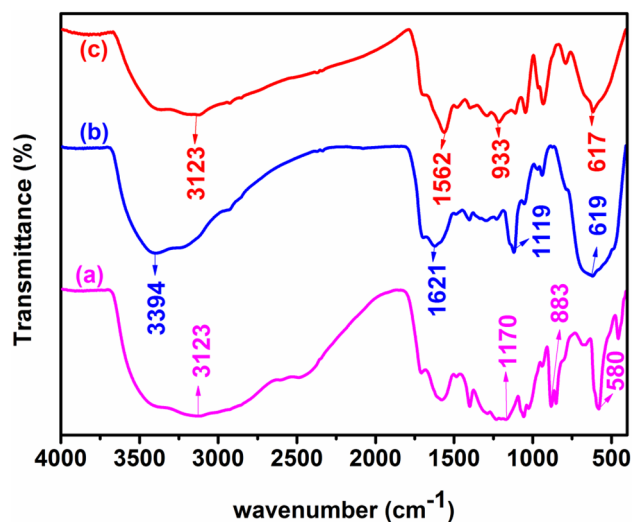

Fig. 1 FTIR spectra of (*a*) PPy (*b*) PPy/SnO$_2$ and (*c*) PPy/Sn nanocomposites

Sn nanocomposites [39]. In Fig. 1a shows the characteristic band of pure PPy, the peak at 1401 cm^{-1} is attributed to N–H stretching of pyrrole ring [40]. The peak at 1182 cm^{-1} corresponds to C–N stretching vibrations [41]. The very strong peaks at 1056 cm^{-1} and 1170 cm^{-1} are attributed to (C–H) in plane vibration [42]. The characteristic peak at 883 cm^{-1} corresponds to C–H out of plane bending vibrations. In the characteristic peak of PPy/Sn nanocomposite at 1562 cm^{-1} is attributed to the pyrrole ring stretching vibrations [43]. The characteristics bands of 1556 cm^{-1} and 933 cm^{-1} can be assigned to C=C bands and N–H in-plane vibrations [44]. In the PPy/SnO$_2$ nanocomposites, the absorption peak at 1621 cm^{-1} is attributed to the bending vibration of water molecules [45]. The FT-IR peaks acquired are in good agreement with the reported literatures. The interaction between PPy and nanocomposites may promote the charge separation and therefore be able to enhance the electron transport property of PPy/SnO$_2$ and PPy/Sn.

3.2 XRD Analysis

Figure 2a–c shows the XRD patterns of PPy, PPy/SnO$_2$ and PPy/Sn nanocomposites. In Fig. 2a, the XRD spectra showed that the PPy was amorphous in nature. The broad amorphous diffraction peak which appears at 2θ = 22.85° [46]. In Fig. 2c shows that the XRD pattern of PPy/Sn. The sharp peaks are at about 30.49°, 31.90°, 43.73°, 44.76° and 55.33° can be associated with (200), (101), (220), (211) and (301) respectively, which attributed clearly Sn nano particle are existing in PPy matrix. XRD spectra showed that the PPy/Sn is crystalline in nature. This matches well with JCPDS, tin file No. 89-2958. The PPy/Sn nanocomposite shows tetragonal body centered, which are in good agreement with the literature. The average crystallite size for this PPy/Sn is found to be 56 nm. All the strong diffraction peaks of (Fig. 2b) PPy/SnO$_2$ nanocomposite can be perfectly indexed as the tetragonal rutile structure for 2θ values of 26.36°, 33.62°,

37.72°, 51.56°, 54.56°, 57.5°, 61.64°, 64.5°, 65.66°, 71.14° and 78.54° can be associated with (110), (101), (200), (211), (220), (002), (310), (112), (301), (202) and (321) respectively. The crystallite size of the prepared PPy/SnO$_2$ is 27 nm (by using the Voigt curve to fit a peak of FWHM value), which was calculated according to Scherrer equation of d = 0.9λ/ßcosθ (λ is the X-ray wavelength, ß is full width at half maximum value, and θ is the diffraction angle). In the PPy/SnO$_2$ and PPy/Sn nanocomposites form, all major peaks for Sn and SnO$_2$ were observed, suggesting that PPy was deposited on the surface.

3.3 UV–Visible Analysis

The UV–vis spectra of PPy/SnO$_2$ and PPy/Sn nanocomposites are shown in Fig. 3a. The characteristic absorption peaks at 291 nm and 290 nm indicates the π–π* transition of the heteroatom aromatic pyrrole ring. The bandgap energy of the PPy samples was calculated by extrapolating the graphs between hν vs. (αhν)^2 (Fig. 3b) using Tauc's relation (αhν)^n = B (hν–Eg), where, α is the absorption co-efficient, h is the plank's constant, ν is the frequency, B is a constant, Eg is the bandgap energy and n is the number that characterizes the transition process (for direct bandgap n = 2). The calculated bandgap values of the PPy/SnO$_2$ and PPy/Sn nanocomposites are found to be 3.38 and 3.48 eV. From the results, the bandgap decreases with the increase of Sn and SnO$_2$ nanoparticles. The reduction band gap offers rapid electron transport behavior which causes good electrical conductivity.

3.4 Morphology and Elemental Analysis

The morphology of the obtained PPy/SnO$_2$ & PPy/Sn nanocomposites have been performed using FESEM with EDX and the images are displayed in Fig. 4a–d.The high maginification FESEM image obtained the presence of

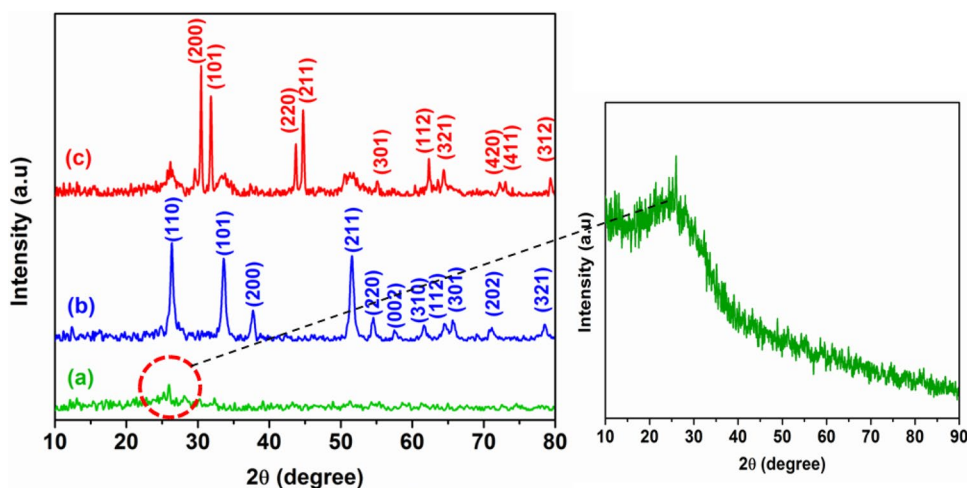**Fig. 2** XRD spectra of (*a*) PPy (*b*) PPy/SnO$_2$ and (*c*) PPy/Sn nanocomposites

Fig. 3 **a** UV–visible spectra and **b** Tauc plot of PPy/SnO$_2$ and PPy/Sn nanocomposites
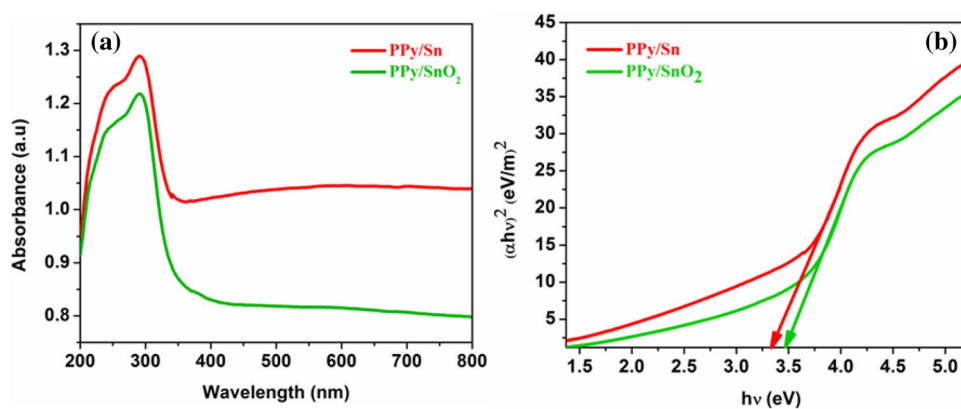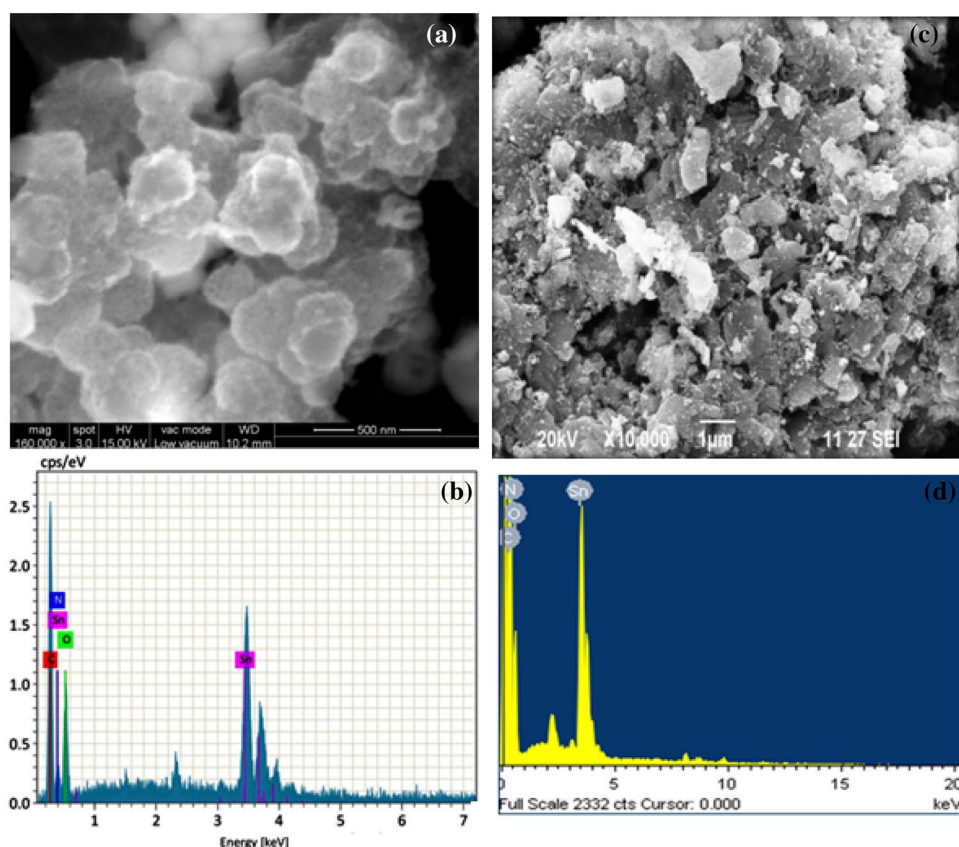

Fig. 4 FESEM and EDX image of **a**, **b** PPy/Sn **c**, **d** PPy/SnO$_2$ nanocomposites

nano tin and SnO$_2$ particles uniformly distributed throughout the nanocomposite sample (PPy/Sn) shows spherical in shape and nano tin particles are embedded in the PPy matrix, whereas the PPy/SnO$_2$ nanocomposite were found to be irregular in shape and there is some agglomeration appeared in the image. In order to further confirm the presence of Sn and SnO$_2$ nanoparticle, energy dispersive X-ray (EDX) spectroscopy was used to observe the elements such as C, O, N and Sn in the nanocomposites are shown in Fig. 4b, d.

3.5 HR-TEM Analysis

The HRTEM micrographs and SAED pattern of the synthesized nanocomposites are displayed in Fig. 5a–d, suggesting the formation of high-resolution (HR-TEM) investigations give further insight into the morphologies and the structural features of PPy/Sn and PPy/SnO$_2$ nanocomposites. The obvious contrast between the dark edge and the pale center of the spheres confirms PPy/Sn nanocomposite hollow nanosphere nature from Fig. 5c [47]. Meanwhile the SnO$_2$ blended PPy shown some agglomerations appeared in
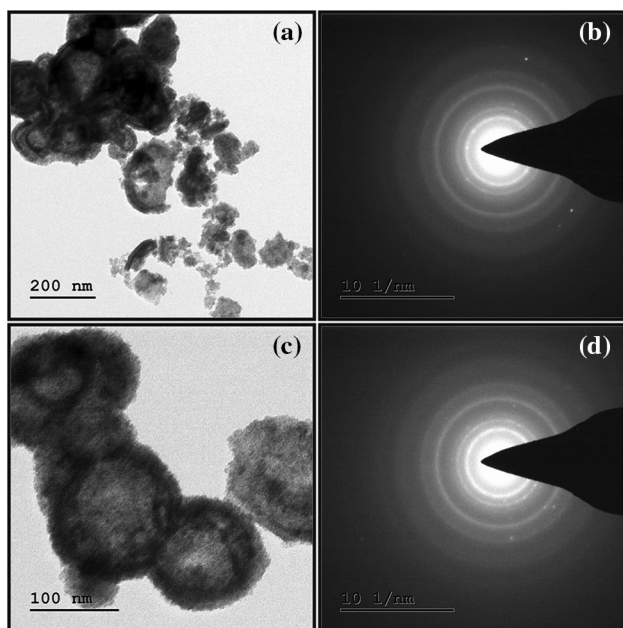
Fig. 5 TEM image of **a**, **b** PPy/SnO$_2$ and **c**, **d** PPy/Sn nanocomposites

the image. One can see its hollow structure and clear grain boundary on the surface. It suggests that the as-obtained hollow sphere is constituted by aggregation of small Sn nano particles, which is in good agreement with the XRD patterns. The hollow structured sphere may the reason for boost the electric conducting property of PPy/Sn nanocomposites.

3.6 Electrical Transport Property

Figure 6a displays AC electrical conductivity of PPy, PPy/SnO$_2$ and PPy/Sn nanocomposites at room temperature. Conductivity measurements have been performed by a typical two probe technique. The AC conductivity of (Fig. 6b) pure PPy is 6.7×10^{-5} S/cm, where as the conductivity of PPy/Sn is 5.2×10^{-1} S/cm and PPy/SnO$_2$ is 3.9×10^{-1} S/cm. The results revealed at lower frequency region the conductivity is constant, at some point the frequency increases as well
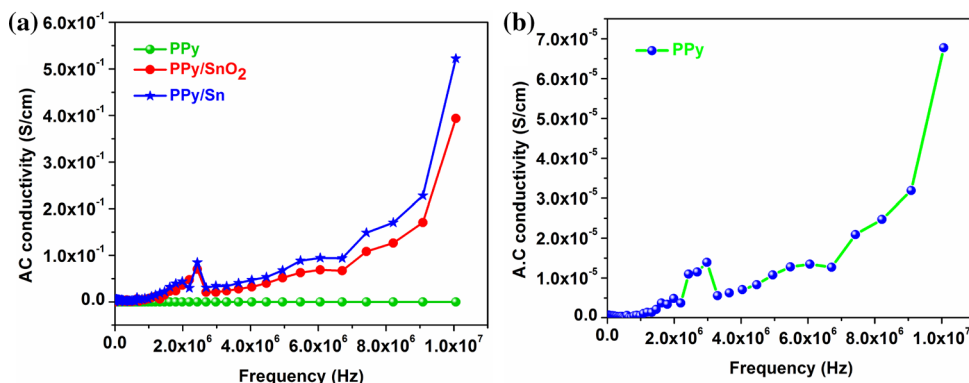
as AC conductivity also improved, it might be the reason of hopping of charge carriers [48]. As we compare to the AC conductivities of pure PPy with PPy/Sn and PPy/SnO$_2$, the conductivity has been increased by four order increase in AC conductivity. The result shows that nano composite posses better electrical conductivity than pure PPy. This enhanced conductivity of PPy/Sn is due to the combination of amorphous and crystalline structure. In accordance to the ordered hollow nanosphere of PPy/Sn nanocomposite, more efficient network for charging in the PPy matrix might result in increased conductivity.

The DC conductivity is decreased when increase of frequency. The frequency dependent dielectric constant was observed in Fig. 7a. At lower frequency the dielectric constant decreases with increase in frequency. At higher frequencies the dipoles follow the field and dipolar polarization the dielectric constant value is very low nearer to zero. The dielectric constant is high due to the accumulation of charges at the boundaries.

4 Conclusion

Nano tin and tin oxide blended with Polypyrrole (PPy/Sn and PPy/SnO$_2$) were synthesized by adopting a facile chemical oxidation polymerization method. The XRD pattern shows that the PPy and PPy/Sn and PPy/SnO$_2$ are amorphous and crystallite in nature respectively. The average crystallite size of PPy/SnO$_2$ and PPy/Sn was found to be 27 and 56 nm. The FESEM and HRTEM morphology showed that the nanocomposites are hollow nanosphere due to the presence of Sn nanoparticle and EDX study reveals that the Sn nanocomposite is evenly distributed throughout the polymer matrix. The FT-IR and UV–vis analysis confirmed the PPy/Sn and PPy/SnO$_2$ nanocomposites. The dielectric constant decreases with increase in frequency of PPy, PPy/SnO$_2$ and PPy/Sn. The achieved results showed that the PPy/Sn has better electrical conductivity than pure PPy and PPy/SnO$_2$ indicated the incorporation of tin nanocomposite in the polypyrrole sample.

Fig. 6 Comparison of A.C Conductivity of pure **a** PPy, PPy/SnO$_2$ and PPy/Sn nanocomposites **b** pure PPy

Fig. 7 Comparison of **a** dielectric constant and **b** DC conductivity of pure PPy, PPy/SnO$_2$ and PPy/Sn nanocomposites
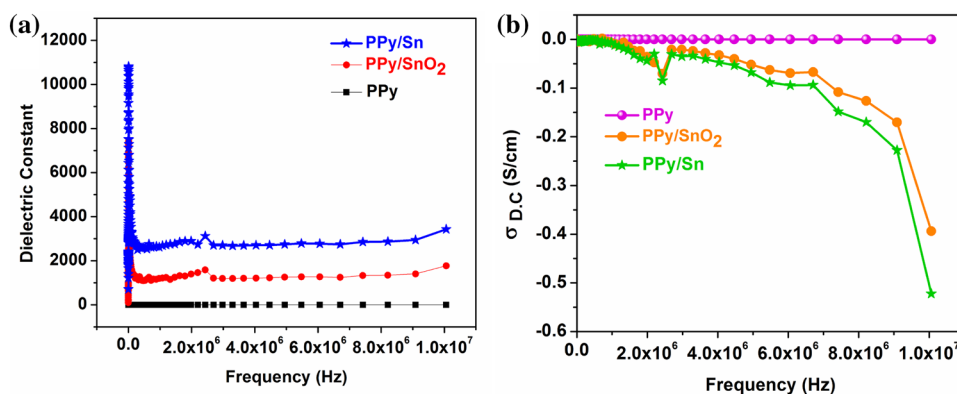
Complaince with Ethical Standards

Conflict of interest The authors declare that they have no conflict of interest.

References

1. H.C. Pant, M.K. Patra, S.C. Negi, A. Bhatia, S.R. Vadera, N. Kumar, Bull. Mater. Sci. **29**, 379 (2006)
2. G.D. Khuspe, S.T. Navale, D.K. Bandgar, R.D. Sakhare, M.A. Chougule, V.B. Patil, Electron. Mater. Lett. **10**, 191 (2014)
3. B.K. Sharma, A.K. Gupta, N. Khare, S.K. Dhawan, H.C. Gupta, Synth. Met. **159**, 391 (2009)
4. T. Abdiryim, R. Jamal, I. Nurulla, J. Appl. Polym. Sci. **105**, 576 (2007)
5. M. Joulazadeh, A.H. Navarchian, Synth. Met. **210**, 404 (2015)
6. J.-H. Kim, A.K. Sharma, Y.-S. Lee, Mater. Lett. **60**, 1697 (2006)
7. S. Walkiewicz, A. Michalska, K. Maksymiuk, Electroanalysis **17**, 1269 (2005)
8. G. Han, J. Yuan, G. Shi, F. Wei, Thin Solid Films **474**, 64 (2005)
9. M.S. Kim, H.K. Kim, S.W. Byun, S.H. Jeong, Y.K. Hong, J.S. Joo, K.T. Song, J.K. Kim, C.J. Lee, J.Y. Lee, Synth. Met. **126**, 233 (2002)
10. Ö. Yavuz, M.K. Ram, M. Aldissi, P. Poddar, H. Srikanth, Synth. Met. **151**, 211 (2005)
11. W. Prissanaroon, L. Ruangchuay, A. Sirivat, J. Schwank, Synth. Met. **114**, 65 (2000)
12. S. Chen, I. Zhitomirsky, Mater. Lett. **125**, 92 (2014)
13. K. Leonavicius, A. Ramanaviciene, A. Ramanavicius, Langmuir **27**, 10970 (2011)
14. A. Kausaite-Minkstimiene, V. Mazeiko, A. Ramanaviciene, A. Ramanavicius, Colloids Surf. A **483**, 224 (2015)
15. F. Ghamouss, A. Brugère, A.C. Anbalagan, B. Schmaltz, E. Luais, F. Tran-Van, Synth. Met. **168**, 9 (2013)
16. Y. Qiao, L. Shen, M. Wu, Y. Guo, S. Meng, Mater. Lett. **126**, 185 (2014)
17. Y. Shi, L. Pan, B. Liu, Y. Wang, Y. Cui, Z. Bao, G. Yu, J. Mater. Chem. A **2**, 6086 (2014)
18. G. Qi, Z. Wu, H. Wang, J. Mater. Chem. C **1**, 7102 (2013)
19. S.-J. Su, N. Kuramoto, Synth. Met. **114**, 147 (2000)
20. S. Pethkar, R. Patil, J. Kher, K. Vijayamohanan, Thin Solid Films **349**, 105 (1999)
21. K.R. Reddy, K.P. Lee, A.I. Gopalan, Colloids Surf. A Physicochem Eng Asp **320**, 49 (2008)
22. L. Jin, S.-P. Yang, Q.-W. Tian, H.-X. Wu, Y.-J. Cai, Mater. Chem. Phys. **112**, 977 (2008)
23. R. Sarathi, T.K. Sindhu, S.R. Chakravarthy, A. Sharma, K.V. Nagesh, J. Alloy. Compd. **475**, 658 (2009)
24. C. Yu, J. Zhai, Z. Li, M. Wan, M. Gao, L. Jiang, Thin Solid Films **516**, 5107 (2008)
25. J. Li, L. Zhu, Y. Wu, Y. Harima, A. Zhang, H. Tang, Polymer **47**, 7361 (2006)
26. J. Arjomandi, S. Tadayyonfar, Polym. Compos. **35**, 351 (2014)
27. M.H. Parvin, M. Pirnia, J. Arjomandi, Electrochim. Acta **185**, 276 (2015)
28. J. Arjomandi, N. Keramat Irad Mossa, B. Jaleh, J. Appl. Polym. Sci. **132**, 41526 (2015)
29. A.G. Yavuz, A. Gök, Synth. Met. **157**, 235 (2007)
30. G. Song, J. Han, R. Guo, Synth. Met. **157**, 170 (2007)
31. L.-Y. Hsiao, J.-G. Duh, J. Electron. Mater. **35**, 1755 (2006)
32. C.Y. Lin, U.S. Mohanty, J.H. Chou, J. Alloy. Compd. **501**, 204 (2010)
33. Y.H. Jo, J.C. Park, J.U. Bang, H. Song, H.M. Lee, J. Nanosci. Nanotechnol. **11**, 1037 (2011)
34. C. Nayral, T. Ould-Ely, A. Maisonnat, B. Chaudret, P. Fau, L. Lescouzères, A. Peyre-Lavigne, Adv. Mater. **11**, 61 (1999)
35. E.R. Leite, I.T. Weber, E. Longo, J.A. Varela, Adv. Mater. **12**, 965 (2000)
36. F. Chen, M. Liu, Chem. Commun. **18**, 1829–1830 (1999)
37. Y. Fukai, Y. Kondo, S. Mori, E. Suzuki, Electrochem. Commun. **9**, 1439 (2007)
38. M.R. Mahmoudian, W.J. Basirun, Y. Alias, Prog. Org. Coat. **71**, 56 (2011)
39. B. Ruan, H. Guo, Q. Liu, D. Shi, S. Chou, H. Liu, G. Chen, J. Wang, RSC Adv. **6**, 103124 (2016)
40. S. Jamadade, S.V. Jadhav, V. Puri, J. Non-Cryst. Solids **357**, 1177 (2011)
41. C.S. Priya, G. Velraj, Mater. Lett. **77**, 29 (2012)
42. J. Zhang, S. Wang, M. Xu, Y. Wang, H. Xia, S. Zhang, X. Guo, S. Wu, J. Phys. Chem. C **113**, 1662 (2009)
43. M.J. Antony, M. Jayakannan, J. Phys. Chem. B **111**, 12772 (2007)
44. R. Liu, D. Li, C. Wang, N. Li, Q. Li, X. Lü, J.S. Spendelow, G. Wu, Nano Energy **6**, 73 (2014)
45. R. Adnan, N.A. Razana, I.A. Rahman, M.A. Farrukh, J. Chin. Chem. Soc. **57**, 222 (2010)

46. S.S. Barkade, D.V. Pinjari, U.T. Nakate, A.K. Singh, P.R. Gogate, J.B. Naik, S.H. Sonawane, A.B. Pandit, Chem. Eng. Process. **74**, 115 (2013)
47. M. Xu, J. Zhang, S. Wang, X. Guo, H. Xia, Y. Wang, S. Zhang, W. Huang, S. Wu, Sens. Actuators B: Chem. **146**, 8 (2010)
48. S.K. Moosvi, K. Majid, T. Ara, Chem. Phys. **478**, 110 (2016)